14,12

Search for optimal conditions for monolithization of ultra-high-molecular-weight polyethylene reactor powder

© L.P. Myasnikova[1], V.F. Drobotko[2], A.P. Borzenko[2], Yu.M. Boiko[1], V.A. Marikhin[1], S.A. Terekhov[2], M.A. Yagovkina[1]

[1] Ioffe Institute,
St. Petersburg, Russia
[2] Donetsk Institute for Physics and Engineering named after A.A. Galkin,
Donetsk, Ukraine

E-mail: liu2000@mail.ru

Received July 20, 2021
Revised July 20, 2021
Accepted July 22, 2021

In order to clarify the possibility of sintering reactor powders of ultra-high molecular weight polyethylene under pressure at a temperature higher than its equilibrium melting point at atmospheric pressure (T_m^0) without catastrophic changes in the internal structure of particles, a comparative WAXS analysis was carried out of the samples sintered below ($T < T_m^0$) and above ($T > T_m^0$) this temperature and cooled under different conditions. A structural analysis of the X-ray scattering curves recorded in the Bragg-Brentano mode on a 2D Phaser Bruker diffractometer from UHMWPE reactor powders sintered under different conditions was carried out, and the crystallite sizes were calculated. It was found that an increase in the sintering temperature above T_m^0 does not significantly change the crystal structure of the polymer, and the precursors produced can be used for further orientational hardening.

Keywords: ultrahigh molecular weight polyethylene reactor powders, sintering, WAXS.

DOI: 10.21883/PSS.2022.13.52325.164

1. Introduction

Currently a solution-free (dry) method is being actively developed for obtaining high-strength, high-modulus filaments and film tapes of ultra-high-molecular-weight polyethylene (UHMWPE) directly from the synthesis products, the so-called reactor powders. This method is an alternative to the expensive and environmentally unsound the method is to sinter the powder at a temperature below polymer melting temperature, followed by orientation stretching.

The company launched the production of high-strength and high-modulus UHMWPE tapes using dry method and, since 2012, has been producing UHMWPE tapes under Endumax trademark. In terms of strength(2.5 GPa) these tapes are still inferior to the strength of Dyneema fibers(3.6 GPa) produced using gel technology by DSM (The Netherlands). At the same time in laboratory conditions both in Russia [1–3] and abroad [4] oriented UHMWPE filaments with much higher mechanical characteristics have been obtained. So, for example, in the group of prof. S. Rastogi (The Netherlands) UHMWPE film filaments were obtained from a powder synthesized on a single-center post-metallocene catalyst F1 with a tensile strength 4 GPa and elastic modulus of 200 GPa [4]. From UHMWPE reactor powders synthesized in the laboratory of prof. S.S. Ivanchev (ITS RAS, Russia) on a single-site post-metallocene catalyst F-97 at A.F. Ioffe Physical-Technical Institute in Laboratory of Fracture Physics high-strength UHMWPE film threads with tensile strength up to 4.5 GPa and elastic modulus 180 GPa [5] were also obtained.

Despite the progress achieved in obtaining high-strength film threads, their characteristics are still far from theoretical estimates. With elastic modulus 200 GPa the ultimate strength of UHMWPE filaments should be about 20 GPa. Therefore, the search for ways to improve the strength characteristics of oriented UHMWPE filaments continues.

Achievement of high strength characteristics depends on two factors: the structure of the reactor powder particles, which is optimal for orientational stretching, and the possibility of creating strong cohesive bonds between the particles, which prevent premature sample rupture in the course of drawing until the maximum possible degree of elongation is reached.

The optimal structure of nascent powder is considered to be a structure with a minimum number of molecular entanglements, the number of which depends on the polymerization temperature, type of catalyst, and many other synthesis conditions. The strength of the interparticle boundaries is determined by the conditions of powder sintering. In this case it is important to preserve the minimum number of entanglements existed in the original structure.

The purpose of this work was a comparative study of the crystal structure of UHMWPE reactor powder after sintering under pressure above and below the equilibrium polymer melting point (T_m) using X-ray diffraction analysis at large angles.

2. Experimental part

2.1. Materials

The studies were carried out using a reactor powder (RP) UHMWPE-5224, synthesized under laboratory conditions at the Institute of Macromolecular Compounds of the Russian Academy of Sciences (Saint Petersburg) by means of slurry polymerization in toluene according to the method described in [6], using titanium halide phenoxyimine catalysts of a special structure PS-1229, activated with methylaluminoxane. Molecular mass of reactor powder 5224 was $Mw = 3.1 \cdot 10^6$ g/mol, $T_{\text{polym}} = 40^\circ$C, bulk density $\rho_{\text{bulk}} = 0.051$ g/cm^3, fraction $250 < d < 850\,\mu$m. Such powder for studies was selected on the basis of literature data indicating the formation of the optimal structure of UHMWPE RP for solid-phase processing during the UHMWPE synthesis oentanglementsn post-metallocene catalysts [6].

2.2. Preparation of samples

Samples for the study were prepared according to powder metallurgy principle, which has long been used in industry for the processing of high-melting metals, ceramics and insoluble and infusible polymers, such as polytetrafluoroethylene, polybenzimidazole, etc. The scheme for preparing initial samples (precursors) for subsequent orientational hardening from UHMWPE RP includes two stages:

1. Compaction of RP at room temperature to create the closest contact between the surfaces of the nearest neighboring UHMWPE RP particles and to increase the adhesion strength of the compact due to the maximum possible reduction of free volume and expulsion of „trapped“ air.

2. Sintering of the obtained compact in order to create the largest number of cohesive bonds between the initial RP particles, providing the mechanical precursor strength, that further allows strain hardening of the precursor by high-temperature multistage orientational drawing without premature rupture of the oriented sample until it reaches the limiting orientational elongations. Sintering is usually carried out under the simultaneous action of pressure and temperature not exceeding T_m of the initial RP.

At the same time, fundamentally important requirements are put forward to the choice of values of compressive forces at the stage of compaction and increased temperature values and compressive forces at the stage of sintering, at which, during the preparation of the precursor, it is necessary to preserve as much as possible the specific morphology formed during the synthesis of the initial RP.

The first stage is RP compaction, which was carried out in accordance with cold pressing method (at room temperature) using a specially made closed cylindrical mold with an inner diameter 20 mm and with two punches carefully adjusted to the diameter. The end surfaces of plane-parallel punches were polished to a roughness less than 1 μm.

For compacting, 60 mg UHMWPE powder was placed between the punches and the mold was installed in a hydraulic press. The choice of the compression pressure and the duration of the compact under load was carried out taking into account the results of studies [7,8]. In the study [7] the data on the compressibility of commercial UHMWPE powders with molecular weight $Mw > 2 \cdot 10^6$ g/mol, with different bulk density and different sizes and shapes of particles were obtained. The compressibility curves of such powders are the dependences of the relative compaction (the so-called compaction parameter DR) on the compression pressure in the mold. For each unsintered (raw) powder the DR increases with pressure, at first rapidly, and then the rate decreases and the curves achieve plateau. Each powder has its own specific plateau density level, which is less than total material density. It turned out that for all studied powders the plateau was reached at the same external compression pressure of about 100 MPa (10 Kg/mm^2), i.e. at relatively low pressures. This result was also confirmed in the study [8], where the authors investigated UHMWPE reactor powders with the same density 0.961 g/cm^3, molecular weights $Mw = 1.74 \cdot 10^6$ and $1.6 \cdot 10^6$ g/mol and different bulk density 0.057 and 0.206 g/cm^3. The compressibility curves of tablets also reached a linear section at a pressure of about 100 MPa. Obviously, due to the observed plateau phenomenon, there is no advantage in using pressures exceeding 100–200 MPa. To obtain higher densities, it is necessary to change powder characteristics, not the pressure.

Taking into account the results obtained in [7,8], we compacted the RP in the above described mold at room temperature, at pressure of $P = 100$ MPa for 15 min. Then the pressure on the press was released by opening the corresponding valve. At the same time, we paid attention that the rates of pressure rise and release were approximately the same for all tablets. As a result we obtained the initial compacted tablets with a diameter of $D = 20$ mm and a thickness of $h_1 = 0.20$ mm, which slightly increased to $h_2 = 0.215$ mm after aging in a desiccator with moisture-absorbing crumbs at room temperature and atmospheric pressure for 24 hours.

The second stage is sintering of compacted RPs, was carried out at a pressure of 100 MPa under various conditions.

Prior to describing the specific conditions for preparing sintered samples for X-ray diffraction analysis, let us turn once again to the mechanism of creating a monolithic film from RP. As already mentioned above, the sintering of the compacted powder is carried out to create strong adhesion between RP particles and to obtain a mechanically strong precursor for orientation hardening. „Healing“ of interparticle boundaries is achieved due to the formation of the molecules between particles in the process of diffusion penetration of free end segments of macromolecules from neighboring contacting particles into each other. On the one hand, to increase molecular mobility and accelerate diffusion, it is desirable to significantly increase the sintering temperature; however, this may lead to an undesirable

rearrangement of the initial supramolecular RP structure or even remelting of the polymer, if sintering is carried out at a temperature above the polymer melting temperature $T \geq T_m^0$. Therefore, sintering is always performed at temperatures below T_m^0 [9].

However, in a number of experimental studies, an increase in polymer melting temperature with an increase in hydrostatic pressure was found. So in the studies [10] and [11] when studying the natural rubber crystallization kinetics, using dilatometric methods for an wide range of temperatures and hydrostatic pressures up to 1100 atm and 2000 atm, the influence of pressure on melting temperature was determined. For this purpose, the differential form of Clapeyron-Clausius equation was used. For natural rubber, it can be expressed as

$$dT_m^0/dP = (dT_m^0 \Delta v)/\Delta H_u = 0.0465\,\text{deg/atm}, \qquad (1)$$

where $\Delta H_u = 15.3$ cal/g stand for latent melting heat, $T_m^0 = 301^\circ$ K is the melting temperature at atmospheric pressure and $\Delta v_u = 0.098\,\text{cm}^3/\text{g}$ is the change in volume per repeating unit of melting.

In the studies [12] and [13] the processes of crystallization and annealing of polyethylene at high pressure, more than 2000 atm were studied. For polyethylene the latent melting heat ΔH_u equal to 68.0 cal/g, $T_m^0 = 410^\circ$ K and $\Delta v_u = 0.16\,\text{cm}^3/\text{g}$ was found. Then $dT_m^0/dP = 0.0235$ deg./atm. Thus, at a pressure of 100 MPa the melting temperature will exceed the melting temperature at atmospheric pressure $\Delta T = T_m - T_m^0$ for polyethylene by 23.5°C and by 46.5°C for natural rubber. Wunderlich [14], analyzing the available literature data for T_m PE at pressures up to$P = 6\,103$ atm, found that the dependence of T_m on pressure can be described by the quadratic equation

$$T_m = 415.7 + 28.1P - 1.66P^2, \qquad (2)$$

where pressure P is expressed in 10^3 atm, and the temperature — is in Kelvin degrees. At the lowest pressures, the slope of this dependence is $35.2\,\text{K}/10^3$ atm, i.e. at $P = 100$ MPa the increase of RP melting temperature can be about $\Delta T_m = 35$ K. There are many theories describing the change of molecules mobility in polymers under pressure. A modern analysis of all existing theories is given in Skorodumov's doctoral thesis [15], which also shows that the melting temperature T_m of polymers under hydrostatic pressure 100 MPa increases by 20–40°C.

Therefore, we assumed that the sintering of compacted tablets under 100 MPa pressure, at a temperature of 145°C, that is slightly higher than the equilibrium T_m^0 at atmospheric pressure (according to our DSC data for UHMWPE RP 5224 $T_m^0 = 141.5^\circ$C) will not lead to a catastrophic change in the internal RP structure, but will provide a more effective interdiffusion of molecular segments on the particles boundaries. To confirm this hypothesis and carry out a comparative analysis of the crystal structure formed during compact sintering at 130°C (standard procedure) and 145°C, the following samples were prepared.

1. The tablet was placed in a mold preheated up to 130°C, at this temperature the pressure was raised up to 100 MPa and kept in the mold for $t = 30$ min. Then the pressure was released, the tablet was removed and cooled to room temperature by placing the tablet between two metal plates (Standard).

2. The tablet was placed in the mold heated up to 130°C and the pressure was raised up to 100 MPa. Then the mold was additionally heated up to 145°C and kept under these conditions for $t = 30$ min. Then the mold was cooled down to 130°C and the pressure was released, the tablet was removed and quickly cooled to room temperature (mode I).

3. The samples in mode II were prepared in the same way as samples in mode I, but when the temperature reached 130°C after the pressure was released, the tablet was cooled down to room temperature in a mold.

4. The samples in mode III in contrast to the samples obtained in mode II, were cooled down to room temperature in a mold at a pressure of 100 MPa.

It is important to note the need to raise the temperature in the mold up to 145°C only when there is already a tablet in it at a pressure of 100 MPa. When releasing the pressure the temperature should not exceed 130°C. Finding a tablet directly in a mold, heated up to 145°C with no pressure, results in catastrophic changes in the structure even within a few seconds necessary to raise the pressure, that is confirmed by our studies of sintered compacts using DSC method [16].

2.3. Wide-angle X-ray diffractometry (WAXS)

Diffraction curves in a wide angular range in scanning mode θ–2θ from sintered compacts were obtained on a D2Phaser powder X-ray diffractometer by Bruker equipped with a copper tube and a PSD detector LynxEye.

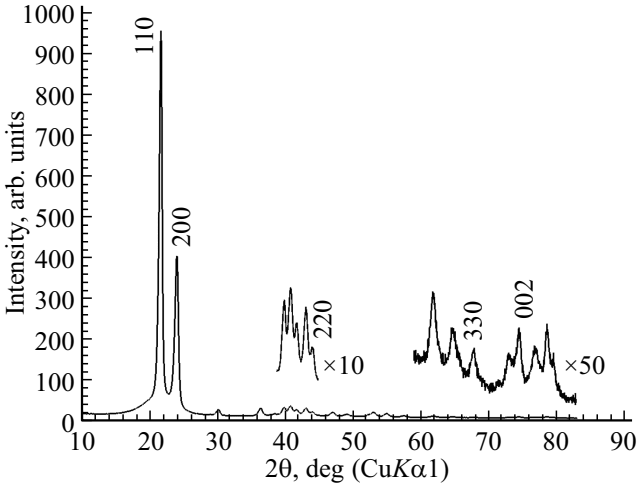

Figure 1. X-ray wide-angle diffraction curve of the initial sintered tablet of UHMWPE-5224 powder.

Fig. 1 shows an X-ray pattern in the range of angles 10−84 degrees on 2θ scale from a sintered tablet of UHMWPE reactor powder obtained according to the standard mode ($T = 130°C$ and $P = 100$ MPa). Since the diffraction curve of orthorhombic polyethylene is represented by only two bright reflections from planes (110) and (200), and the remaining reflections have a very weak intensity, in Fig. 1 the individual intervals on an enlarged scale on the intensity scale are shown. The intensity within the interval for reflection (220) is increased by 10 times, and for (330) and (002) — by 50 times.

2.4. Methods for calculating the size and distortion of crystallites

2.4.1. Scherrer method. It is known that when decreasing the size of the regions of coherent scattering of X-rays (crystallites) and the appearance of defects of various types in them, the width of diffraction reflections increases significantly in comparison with the instrumental width for ideal large crystals. Several approaches have been proposed for analyzing the effects of broadening of reflections to estimate the size of crystallites and their defectiveness. The simplest of them — is the Scherrer method [17], which assumes that the broadening is the result of extremely small sizes of crystallites, the internal structure of which is defect-free.

In this approximation the average crystallite sizes D_{hkl} in the direction perpendicular to (hkl) planes are estimated by the formula:

$$D_{\text{hkl}} = k\lambda/(\Delta 2\theta)_t \cos\theta_m, \tag{3}$$

where: θ_m is the angle position of the peak (maximum) reflex, rad.; $(\Delta 2\theta)_t$ is the true linear reflex half-width, rad.; λ is the wavelength of the radiation used; κ is the Scherrer constant, which is most often taken equal to $\kappa = 0.9$. (More details, please see [18]).

A priori we can assert, that this „idealized“ approach allows to obtain only an approximate estimate of the crystallite sizes, which cannot be used to establish the correct structure-property relationships. Unfortunately, due to its simplicity, this method is still used too often.

2.4.2. Williamson-Hall method. The method somewhat expands the capabilities of the Scherrer method, since it considers the additional contribution to the broadening of type I reflections defects caused by the presence of inhomogeneous internal mechanical stresses in the bulk of polycrystalline material. To separate the effects of the grain size dispersion and microdistortions, it is necessary to measure at least three orders of reflection from one plane system and to use different dependences of the dispersity and microdistortions on $\sin\theta/\lambda$. For example, if we assume that the broadening due to dispersity and due to microdistortions is described by Cauchy function, then we can construct a dependence for different orders of reflection in the form

$$\beta = k\lambda/D\cos\theta + \varepsilon 4\tan\theta, \tag{4}$$

where β is the physical broadening of the diffraction maximum; λ is the CuK_α-radiation wave length; K is the Scherrer constant (can be accepted equal to one); D is the size of coherent scattering areas; θ is the Bragg angle; ε is the value of crystal lattice microdistortions.

Let us modify the function (4) as follows

$$\beta\cos\theta = \lambda/D + \varepsilon 4\tan\theta \tag{5}$$

we see that this is the equation of straight line, where the segment cut along the ordinate axis will give the value λ/D. From the obtained linear function $\beta\cos\theta/\lambda$ from $4\sin\theta/\lambda$ we can calculate the values of the average CSR (coherent scattering region) size and ε.

If both functions are of the form $e^{-\alpha x^2}$ (Gaussian functions), then we construct a similar dependence for two or three reflection orders as follows

$$\left((\beta\cos\theta)/\lambda\right)^2 = (K/D_{110})^2 + \left((\varepsilon 4\sin\theta)/\lambda\right)^2, \tag{6}$$

where ε is the value of the crystal lattice microstresses.

2.4.3. Hosemann method. The analysis of diffraction patterns from partially crystalline polymers shows that in comparison, for example, with metals, their X-ray patterns contain significantly fewer reflections, and a significant decrease in the intensity and an increase in the half-width of reflections for long-range orders are observed. These unusual effects were explained by Hosemann [19] on the basis of a new concept — paracrystalline nature of structural elements aggregation in low-order systems and the appearance of type II distortions. In the samples studied by us, such structural elements are mosaic plate-like lamellas consisting of crystallites of folded molecules. In such systems there is no strict periodicity of long-range order in the arrangement of motives, and fluctuations in the distances between the motives appear, which increase with increasing distance from the selected origin and, moreover, affect all other distances. Therefore, the distribution function of the location of neighbors, instead of being ideally periodic in the presence of type I defects, becomes a statistical paracrystalline distribution function of the second kind, in which the distribution of the first neighbors is relatively clearly expressed, i.e. short-range order. The further the motif is located, the more diffuse the distribution function becomes, and at a certain distance (interaction radius, ordering area, paracrystal size) the conditions of coherent scattering of X-rays by a weakly ordered system are violated.

In the Hosemann method[19] the sizes of paracrystals D_{hkl} and the values of paracrystalline distortions g are calculated based on the integral intensities of reflections of several orders.

The integral half-width of $\Delta\beta(b)$ reflection was determined as follows

$$\Delta\beta)(b) = \frac{\int_{b_1}^{\beta_2} I(b)db}{I_{\max}}, \quad (7)$$

where: $I(b)$ is the scattering intensity after background subtraction and instrumental distortions, $I_{\max}$ is the reflection intensity in maximum.

The initial dependence of the reflection intensity on the Bragg scattering angle 2θ was reconstructed as a function of the scattering angle $b = 2\sin\theta/\lambda$, where λ — is the X-ray radiation wavelength, in accordance with the formula

$$\Delta b = \big((2\cos\theta)/\lambda\big)\Delta\theta. \quad (8)$$

In this study for all investigated samples, the sizes of paracrystals and paracrystalline distortions were determined based on the analysis of the integral intensities of three orders of reflections from the planes (110), (220), and (330) for orthorhombic crystalline unit cells.

The integral half-width of reflections of any order from crystal planes (hkl) is related to the size D_{110} of crystallites perpendicular to these planes and the value of paracrystalline distortionsg_{110} by the following expression [19]:

$$\Delta\beta = 1/D_{110} + (\pi g_{110})^2 d_{110} b^2, \quad (9)$$

where d_{110} — is the identity period (or averaged period) in the direction perpendicular to the planes (110), (220) and (330).

If you build a graph in coordinates $\Delta\beta - b^2$, then for three orders of reflection a straight line should be observed, cutting off on the Y-axis a segment equal to $\Delta\beta_0 = 1/D_{110}$. The value of paracrystalline distortions g_{110} is found from the slope of the straight line $\mathrm{tg}\,\alpha$

$$g_{110} = \sqrt{\frac{\mathrm{tg}\,\alpha}{\pi^2 d_{110}}}. \quad (10)$$

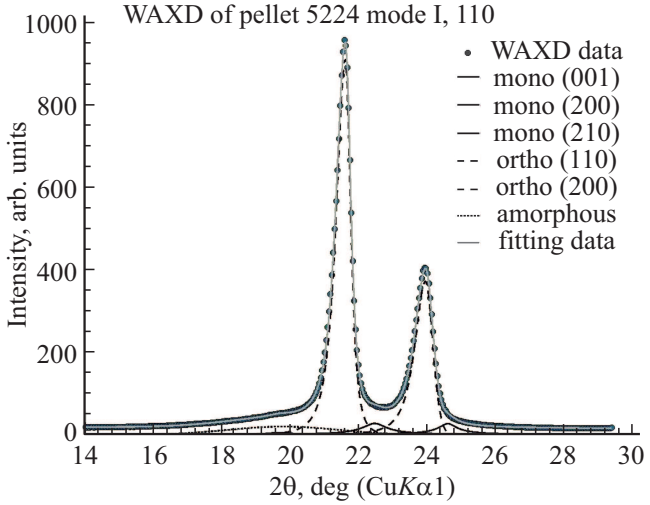

Figure 2. Decomposition of overlapping reflections into components for an experimental diffraction pattern of the first order of reflection (110) within the angular range of 14−28 degrees in 2θ. ($R^2 = 0.99942$, and $\chi^2 = 0.03367$).

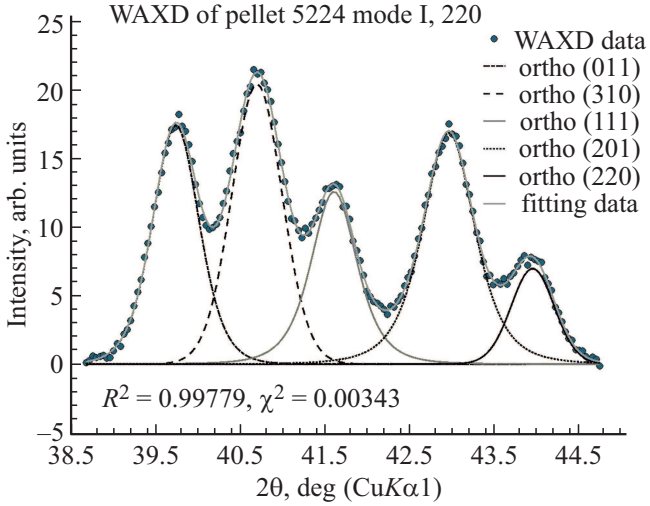

Figure 3. Decomposition of overlapping reflections into components for an experimental diffraction pattern of the second order of reflection (220) within the angle area of 38−45 degrees in 2θ.

3. Results and discussion

As an example Figures 2−4 show three selections of experimental diffraction patterns from sintered reactor powder 5224, obtained by mode I. Several overlapping diffraction maxima are clearly seen in these selections, respectively:

Fig. 2 — diffraction angle area 2θ from 14 to 38 degrees (first orders of reflection from planes (110) and (200) of the orthorhombic cell).

Fig. 3 — diffraction angle area 2θ from 38 to 45 degrees (diffraction peaks of the second order of reflection from planes (220) of the cell, as well as reflections from planes (011), (310), (111) and (201)).

Fig. 4 — diffraction angle area 2θ from 59 to 70 degrees (diffraction peak of the third order of reflection from planes (330), as well as reflections from planes (230), (420), (321) and (411)).

Since in the Hosemann method for further analysis it is necessary to obtain the most correct values of the integral intensities of three orders of reflection from the planes (110), (220), and (330), it was necessary to carry out a computer decomposition of complex diffraction patterns shown in Fig. 2, 3 and 4.

The experimental data were decomposed into individual peaks by fitting the profile functions using LIPRAS MATLAB software [20]. The profile sym-

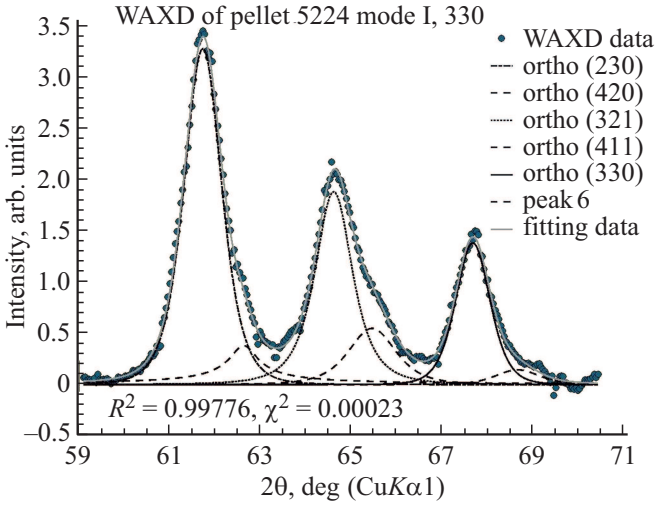

Figure 4. Decomposition of overlapping peaks into components for an experimental diffraction pattern of the third order of reflection (330) in the angle area 2θ 59–69.8°.

metric Gaussian, Pearson-VII and pseudo-Voigt functions were used. The fitting was performed using Trust-Region-ReflectiveLeastSquares and Levenberg–Marquardt algorithms [21]. The quality of fitting and decomposition was assessed by the determination coefficient R^2 and fitting criterion χ^2 (see Fig. 2).

A fragment of an experimental diffraction pattern of the first order of reflection against the background of two large overlapping peaks of the orthorhombic phase $2\theta_{(110)} = 21.47$ deg. and $2\theta_{(200)} = 23.78$ deg. contains a series of low-intensity overlapping peaks of the monoclinic phase: m_{001} ($2\theta = 19.67$ deg.), m_{200} ($2\theta = 22.45$ deg.) and m_{-201} ($2\theta = 24.59$ deg.).

Fig. 3 shows the decomposition of overlapping reflections using the Pearson-VII fitting profile function. The parameter m was close to 10. The diffraction curve in the range of angles 38–45 degrees 2θ contains five peaks related to the orthorhombic phase: (011), (310), (111), (201), (220).

Decomposition of overlapping reflections in the range of angles 59–69.8 degrees in 2θ shown in Fig. 4 contains peaks related only to the orthorhombic phase: (230), (420), (321), (411), (330).

As earlier shown in the literature (see, for example, [22]), for polymer crystals X-ray diffraction data processing using Hosemann method described above in the section „Experimental part“is more correct. If you build a graph in coordinates $\Delta\beta - b^2$, then for three orders there should be a straight line cutting off on the Y-axis a segment equal to $\Delta\beta_0 = 1/D_{110}$. The value of paracrystalline distortions g_{110} is found from the straight line slope tg α.

Indeed, in our case, for all studied samples, a linear dependence $\Delta\beta$ on the squared scattering vector was observed, that indicates that the broadening of the observed reflections is mainly due to the paracrystalline nature of CSR.

The example of such a graph is shown in Fig. 5.

The experimental reflexes were fitted using the Pearson VII profile function, in which the values of index m were close to 10. At these values the Pearson VII function is described as a Gaussian function. At $m \sim 1$ the Pearson function VII is close to the Lorentzian function.

From the analysis of previously published data on polymer samples, it follows that in most cases crystal defects are of a paracrystalline nature and, in rare cases, are caused by internal mechanical stresses [23]. To consider the possibility of microstresses existence in sintered tablets, we calculated the transverse sizes of crystallites and the values of microstresses using Williamson-Hall method described above. For Pearson VII profile function we used the integral broadening correction for the Gaussian profile and we have

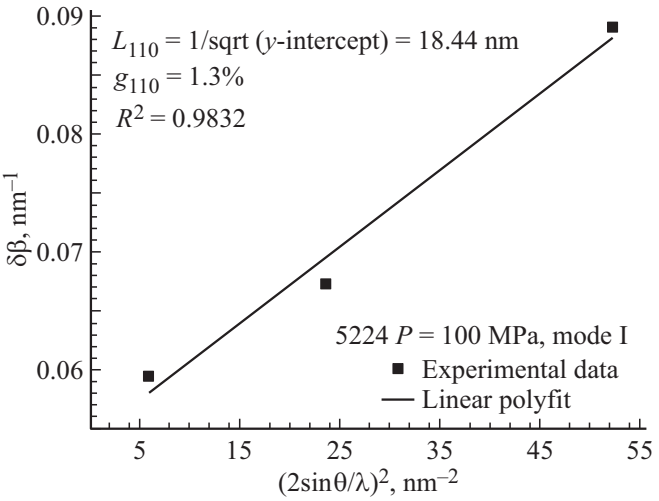

Figure 5. Dependence $\Delta\beta$ (b) on b^2 (formula (9)) for a 5224 tablet sintered at a pressure of 100 MPa and a temperature of 145°C and quickly cooled (mode I).

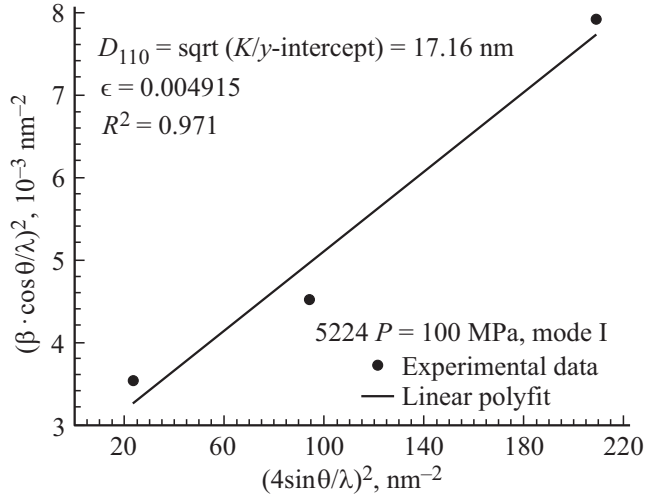

Figure 6. Williamson-Hall approximation (formula 6) for a tablet 5224 sintered at a pressure of 100 MPa and a temperature of 145°C and quickly cooled (mode I).

Table 1. Summary table of crystallite sizes and lattice distortions in UHMWPE samples of 5224 series prepared at different sintering modes

Sample	Method Hosemann				Williamson-Hall approach		
	D_{110}, nm	D_{002}, nm	g_{110},%	R^2	D_{110}, nm	ε	R^2
Mode I	18.44	11.40	1.3	0.9832	17.16	0.00491	0.9711
Mode II	16.17	10.03	0.85	0.9956	14.48	0.00323	0.9920
Mode III	18.18	10.01	1.4	0.9624	17.24	0.00547	0.9477
Standard	17.76	9.76	1.6	0.8955	17.83	0.00667	0.8896

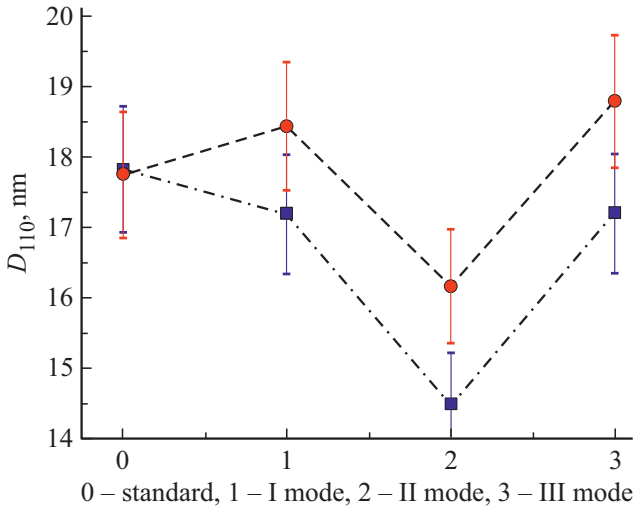

Figure 7. The sizes of crystallites D_{110} in sintered tablets of UHMWPE RP 5224 prepared under different conditions. Calculation according to paracrystalline model (dashed line), calculation according to W_H (dash-dotted line).

built the shown in Fig. 6 graph according to formula (8) (from Cauchy equation (5), it differs as a graph with coordinates „squared").

Let us demonstrate a summary Table 1 crystallite sizes D_{110} in nm, paracrystalline distortions g_{110} (in %) and value ε of lattice microstresses for crystallites perpendicular to the planes (110), (220) and (330) for a standard sample and three modes of sintering 5224 powder tablets, calculated by two methods: Hosemann and Williamson–Hall methods. The crystallite size D_{002} in the direction perpendicular to the plane (002) was determined under the assumption that the value of paracrystalline distortions is $g = 0$.

For greater clarity the sizes of crystallites D_{110} calculated using the paracrystal (Hosenann) model and assuming the predominant influence of microstresses on broadening of (W−H) reflections, are shown in Fig. 7 graphically.

The sizes of crystallites D_{110} calculated according to Williamson–Hall method, turned out to be 7.5%−11.7% smaller depending on the cooling modes at close values in the initial samples with the Hosemann method.

Table 2. Parameters of the orthorhombic crystal cell of UHMWPE 5224 powders sintered under a pressure 100 MPa under different conditions

Sintering	a, (±0.004) nm	b, (±0.004) nm	c, (±0.004) nm
Mode I	0.748	0.496	0.255
Mode II	0.748	0.497	0.255
Mode III	0.750	0.497	0.255
Standard	0.750	0.498	0.255

It is important to note that the sintering at polyethylene temperatures above T_m^0 under the conditions of modes I and III results in insignificant increase of the transverse size of crystallites D_{110} by 3.8−2.7% (depending on cooling conditions) compared with a standard sample sintered at $T < T_m^0$. However, in the tablets made according to mode II (slow cooling in a mold without pressure) the value of D_{110} turns out to be noticeably less than in a standard sample (by 9.8%).

It is currently not possible to say unambiguously about the cause of the observed effect. However, the analysis of the data obtained during the processing of powdered polymers and published in [24] allowed us to assume, that upon slow cooling of UHMWPE RP tablet (mode II) without pressure to room temperature in disordered areas at the boundaries between powder particles the secondary crystallization takes place. The sizes of these newly formed crystallites appear to be smaller than those of the groundmass due to limited space and lack of material. Along with this the primary crystallites are improved and the distortions in them are reduced. The appearance of small crystallites and the improvement of the previously formed CSR results in smaller CSR sizes in the samples obtained in mode II.

From Table 1 it also follows that sintering at 145°C is accompanied by a decrease in the defectiveness of the crystal lattice. The values of paracrystalline distortions g_{110} calculated in the Hosemann paracrystalline model for all three samples sintered in different modes at 145°C are smaller than the paracrystalline distortions in the standard sample sintered at 130°C, that is especially noticeable in

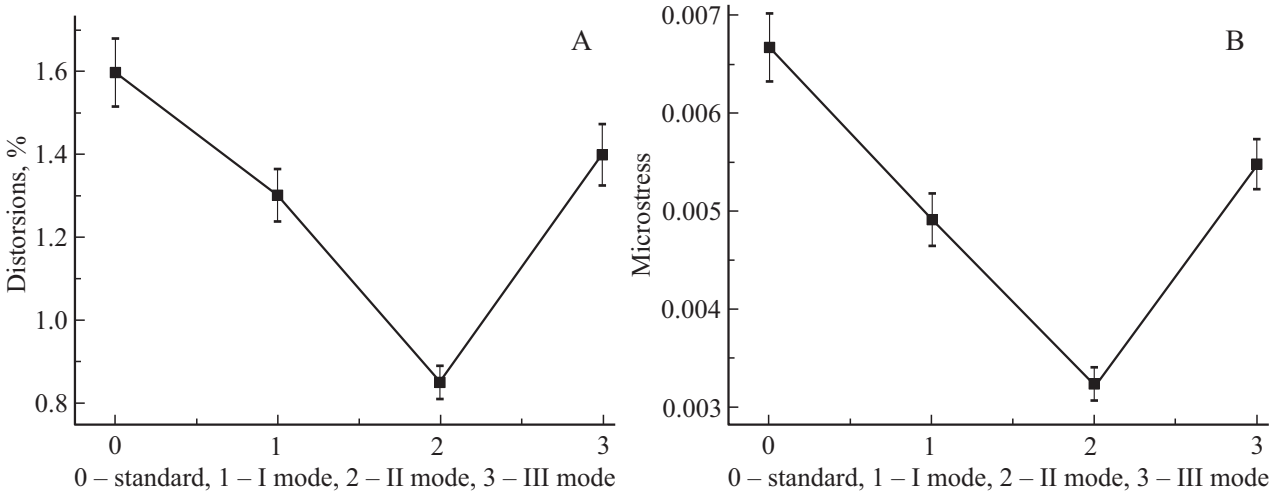

Figure 8. Paracrystalline distortions (A) and microstresses (B) of the studied samples.

sample II (Fig. 8, the left part). Microstresses repeat the same dependence from sample to sample.

The sizes of unit cell a, b and c of orthorhombic crystals calculated from wide-angle experimental X-ray diffraction pattern are given in Table 2.

The unit cell sizes a, b and c for all three sintering modes remain constant within the experimental measurement error.

4. Conclusion

A comparative X-ray diffraction analysis of UHMWPE powders sintered at the temperatures below and above the equilibrium melting temperature of polyethylene at atmospheric pressure (T_m^0) was carried out. The sizes of crystallites are calculated in the directions perpendicular to the crystallographic planes (110) and (002). It was found that a noticeable decrease in the transverse sizes of crystallites (D_{110}) compared to their sizes in standard samples sintered at $T < T_m^0$ is observed only in the samples that cooled after sintering in a press without pressure (mode II). The calculations were performed using the Hosemann paracrystal model and the Williamson–Hall method. The crystallite sizes D_{110}, calculated under the assumption of the paracrystalline structure of the order areas, for all studied samples were 20% higher than those calculated under the assumption of broadening of reflections due to microstresses. This does not change the above conclusion, but requires further analysis taking into account the presence of reflections of the metastable monoclinic phase existing only under voltage. The longitudinal sizes of crystallites (D_{002}) are also practically independent of the sintering temperature. The only exception is the powder quickly cooled after sintering (mode I), in which the value D_{002} turned out to be 14% higher than that of the rest of the samples.

It is concluded that sintering UHMWPE reactor powders under a pressure of 100 MPa at $T > T_m^0$ does not lead to significant changes in the polymer crystal structure and they can be used as precursors for orientational hardening of the material. Further study of the precursors deformation-strength properties will show whether an increase in compacts sintering temperature effective for increasing the strength of interparticle boundaries.

Work funding

The study was carried out with support from the Russian Foundation for Fundamental Research (project codes 19-03-00789, 19-29-12049 and 18-29-17023mk).

Conflict of interest

The authors declare that they have no conflict of interest.

References

[1] M.B. Konstantinopolskaya, S.N. Chvalun, V.I. Selikhova, A.N. Ozerin, Yu.A. Zubov, N.F. Bakeev. Vysokomolekulyarn. soedineneniya (in Russian) **27 A**, 538 (1985).
[2] V.I. Selikhova, Yu.A. Zubov, E.A. Sinevich, S.N. Chvalun, N.I. Ivancheva, O.V. Smol'yanova, S.S. Ivanchev, N.F. Bakeev. Vysokomolekulyarn. soedineneniya (in Russian) **34A**, 92 (1992).
[3] E.A. Sinevich, V.A. Aulov, N.F. Bakeev. Vysokomolekulyarn. soedineneniya (in Russian) **50A**, 1515 (2008).
[4] S. Rastogi, Y. Yao, S. Ronca, J. Bos, J. Van der Eem. Macromolecules **44**, 5568 (2011).
[5] V.N. Varyukhin, V.F. Drobot'ko, S.S. Ivanchev, V.A. Marikhin, L.P. Myasnikova, N.E. Pismenova, E.I. Radovanova, S.A. Terekhov, M.A. Yagovkina. Sb. materialov. XXIII Peterburgskie chteniya po problemam prochnosti. Izd-vo VVM (2018). (in Russian) P. 352. ISBN 978-5-9651-1135-0.
[6] S.S. Ivanchev, A.N. Ozerin, N.I. Ivancheva, S.N. Chvalun, I.I. Oleynik, N.F. Bakeev, M.G. Eremeeva, E.V. Sviridova, V.A. Aulov, I.V. Oleynik, A.S. Kechek'ian. Patent RF RU (11) 2 552 636 (13) C2. (in Russian)

[7] G.W. Halldin, I.L. Kamel. Polymer Eng. Sci. **17**, 26 (1977).
[8] V.A. Aulov, S.V. Makarov, I.O. Kuchkina, A.N. Ozerin, N.F. Bakeev. Vysokomolekulyarn. soedineneniya (in Russian) **A42**, 1850 (2000).
[9] L.P. Myansikova, Yu.M. Boiko, V.M. Egorov, E.M. Ivan'kova, D.V. Lebedev, V.A. Marikhin, E.I. Radovanova, G.H. Michler, V. Seidewitz, S. Goerlitz. Chapter 5 pp 93-151 in Reactor Powder Morphology ed. by L. Myasnikova and P.J. Lemstra, Nova Sci. Publ., USA (2011).
[10] D.E. Roberts, L. Mandelkern. J. Am. Chem. Soc. **77**, 786 (1955).
[11] G.M. Martin, L. Mandelkern. J. Appl. Phys. **34**, 2317 (1963).
[12] J. Osugi, K. Hara, N. Hirai, J. Hikasa. Rev. Phys. Chem. Jpn **34**, 64 (1965).
[13] R. Wunderlich, T. Arakawa. J. Polym. Sci. A, **2**, 3706 (1964).
[14] B. Wunderlich. Macromolecular physics. Crystal nucleation, growth, annealing. Academic Press, N.Y. (1976). V. 2. 560 p.
[15] V.F. Skorodumov. Doctoral thesis by Dr. Phys.-Math. Sci. M. (2010). 419 p.
[16] L.P. Myasnikova, V.F. Drobot'ko, A.P. Borzenko, N.E. Pis'menova, E.M. Radovanova, Yu.M. Boyko, V.A. Marikhin, A.K. Borisov, V.M. Egorov. Sb.: Aktual'nye problemy prochnosti. (in Russian) Vitebsk (2020).
[17] J.I. Langford, D. Loufir. Rep. Prog. Phys. **59**, 131 (1996).
[18] Modern Powder Diffraction / Ed. D. Bish, Post J. Chelsea. Michigan: Mineralogical Society of America 20 (1989).
[19] R. Hosemann, W. Wilke. Makromol. Chem. **118**, 249 (1968).
[20] G. Esteves, K. Ramos, C.M. Fancher, J.L. Jones. LIPRAS: Line-profile Analysis Software (2017); DOI: 10.13140/RG.2.2.29970.25282/3.
[21] https://www.mathworks.com/help/optim/ug/least-squares-model-fitting-algorithms.html.
[22] Yu.M. Boyko, K. Stahl, V.A. Marikhin, L.P. Myasnikova. Vysokomolekulyarn. soedineneniya (in Russian) **9A**, 1992 (2007).
[23] Yu.A. Zubov, V.I. Selikhova, V.A. Kargin. Vysokomolekulyarn. soedineneniya (in Russian) **9A**, 364 (1967).
[24] L.A. Igonin Vysokomolekulyarn. Soedineneniya (in Russian) **10A**, 2726 (1968).